Aerodynamical Resistance in Cycling
CFD Simulations and Comparison with Experiments

Luca Oggiano, Live Spurkland, Lars Sætran and Lars Morten Bardal

Norwegian University Of Science and Technology, Deparment of Energy and Process Engineering,
K. Hejes Vei 2b, 7042 Trondheim, Norway

Keywords: Aerodynamics, CFD, Wind Tunnel Testing, Cycling.

Abstract: The present work shows a comparison between computational fluid dynamics (CFD) simulations obtained using the Unsteady Reynolds Averaged Navier-Stokes solver STARCCM+ from CD-Adapco and experiments carried out in the subsonic wind tunnel at NTNU. The models tested in the wind tunnel (a mannequin and real cyclist in static position) were 3D scanned using a 3D scanner, consisting 48 single-lens reflex cameras surrounding the object in three heights (low/ground-midi-above). A hybrid meshing technique was used in order to discretize the surface and the volume. Polyhedral cells were used on the model surface and in the near volume while a structured grid was used in the rest of the domain. An unsdeady RANS approach was used and the turbulence was modelled using the Menter implementation of the k-ω model. No wall functions were used and the boundary layer was fully resolved. The first part of the paper focuses on the mannequin while in the second part the comparison between the experimental results and simulation on the real cyclist are presented. An overall good agreement between the simulations and the experiments was found proving that CFD could be a complementary tool to wind tunnel testing.

1 INTRODUCTION

The aerodynamic drag is the main opposing force that cyclists need to overcome and it counts up 90% ((De Groot et al., 1995, Di Prampero, 2000; Oggiano et al., 2008)) of the total resisting forces experienced by a cyclist at racing speeds. The cyclist itself counts up to 70% of the total drag while the remaining 30% is due to the bicycle (Blocken et al., 2013; Underwood, 2012; Underwood and Jermy, 2011; Oggiano et al., 2008) and this leads to the fact that even small reductions could give large improvements in terms of performances.

The aerodynamic drag generated by the cyclist is directly linked to a number of parameters.

Expressing the drag as

$$F_D = 0.5 c_D \rho U^2 A \qquad (1)$$

It can be immediately noticed that, for a given location where the air density ρ [kg/m^3] is assumed to be constant, the drag is proportional to the square of the wind speed U [m/s], to the frontal area A [m^2] and to the non-dimensional drag coefficient C_D [-].

Being the frontal area measurements often not reliable (Debraux et al., 2012), a combined

parameter called arag area $C_D A$ is used to quantify the effectiveness of a cycling posture.

In order optimize their posture with the main goal to reduce the drag area (and thus the drag), experimental tests became common amongst elite cyclists. Different methods of assessment of aerodynamic drag (wind tunnel tests, linear regression analysis models, traction resistance measurement methods and deceleration methods) are currently used and each of them has pros and cons (Debraux et al., 2012).

Beside experimental methods, Computational Fludi Dynamics (CFD) simulations became a viable option due the increase in computational power available and to the possibility to parallelize the simulations splitting large meshes into smaller domains. Encouraging results from CFD simulations applied to cycling can be found in (Hanna, 2002; Defraeye et al., 2010a; Defraeye et al., 2010b; Defraeye et al., 2011; Lukes et al., 2002; Blocken et al., 2013) and while applications in other sports have been carried out by a number of other authors (Lecrivain et al., 2008; Minetti et al., 2009; Zaïdi et al., 2010).

CFD simulations present some pros and some cons if compared with wind tunnel tests. While wind

tunnel tests are able to provide only the total drag force acting on the model, CFD can provide drag information on individual body segments or bicycle components, increasing the insight in drag reduction mechanisms and allowing local modifications. Furthermore, CFD simulations are able to provide instantaneous field data while wind tunnel tests are not. On the other hand, the main disadvantage of CFD versus wind tunnel tests is that moving athletes are extremely complex to simulate and thus simulations are confined to static models. The other main issue is that, in order to reduce the computational cost of the simulations, turbulence has to be modelled and cannot be fully resolved. This simplification has two main drawbacks: the separation lines on the model will be placed considering the flow around the model fully turbulent (not always true in reality) and, even with the use of surface roughness and transition models, drag reduction techniques (Oggiano and Sætran, 2012; Oggiano et al., 2009; Brownlie, 1992; Brownlie et al., 1987; Brownlie et al., 2009) cannot be simulated or directly implemented in the simulation.

The present work aims to validate CFD simulations towards experiments proving the effectiveness of CFD as a complementary rather than a substitute tool to wind tunnel tests.

2 EXPERIMENTAL SETUP

Testing of the mannequin models and cyclist were conducted in the large wind tunnel at NTNU. The wind tunnel is equipped with a 220KW fan engine, has a maximum speed of 30m/s and the testing section is 2,7x1,8x12,5 meters. A pitot tube and a thermocouple type K was used to monitor the wind speed and temperature respectively. The drag was measured with a Schenck six component force balance where only the axis of the drag direction was used. The drag force was calculated from the measured CdA values and normalized

2.1 Mannequin Model

The test on the mannequin model were conducted on five velocities ranging from 9.53 to 18.2 m/s (corresponding to 35 to 72,5 km/h).

The mannequin model used for the test was a full-scale upper body including head and upper arms belonging to a model of height 170 cm and weight 70 kg. Its position was adjusted to imitate that of a cyclist in the drop bars. The forearms were removed

to reduce the amount of uncertainty and helmets were not included in the test. The model was tested with a number of jerseys with different surface pattern and without jersey with different rough patches applied to the shoulder. Its position was adjusted to resemble the dropped position of a cyclist.

2.2 Mannequin Model

The full scale test on a cyclist was carried out at a single wind speed (13.09m/s). A regular road bike was placed on a training roller so that the tires were not touching the wind tunnel floor and the roller was connected to the force plate. The front wheel was stationary and supported by a custom-made wheel stand. The cyclist was positioned in drop positon with live pictures from a side camera projected in front of the rider showing their position superimposed with an outline of her initial position to keep it as consequent as possible.

3 NUMERICAL SETUP

3.1 Computational Domain and Geometry
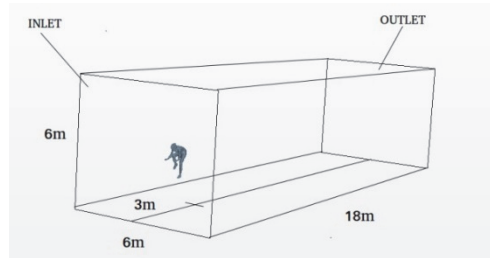
Figure 1: Numerical wind tunnel.

The numerical simulations were set up for a cyclist without bicycle setup and for a mannequin without support setup. The bike modelling was discarded in order to reduce the mesh size and thus the computational cost of the simulation. However, due to this approach, the interaction between the bike and the cyclist was discarded and simplified. No roughness was added to the model while it has been previously shown that roughness could be a key factor and dramatically affect the drag (Brownlie, 1992; Brownlie et al., 1987; Brownlie et al., 2009). The digital models for mannequin and cyclist were obtained using a high-resolution 3D laser scanning. The cyclist and mannequin digital models were placed in a numerical wind tunnel. A

preliminary study on the domain size was carried out in order to avoid backflow that could affect the simulation. The domain shape and size is specified in Figure 1.

3.2 Mesh and Grid Sensitivity
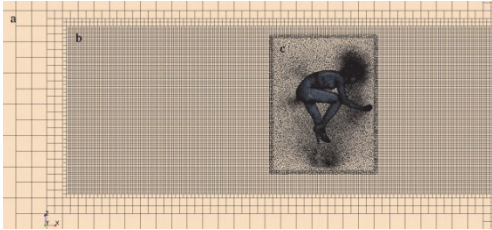
Figure 2: Mesh refinement technique a) farfield area (structured mesh). b) wake area (structured mesh). c) Near model area (unstructured polyhedral mesh).

A hybrid meshing approach was used to mesh the cyclist and the wind tunnel. A polyhedral meshing approach was used to discretize the models surface while a structured hexaedra approach was used for the rest of the domain. The polyhedral meshing technique allows smoother surfaces using fewer cells than triangular and tetrahedral meshing reducing computational cost. The boundary layer was resolved using an extruded mesh consisting of 10 layers. A growing ratio of 1.25 was used and the nearest cell to the surface was placed in order to ensure a non-dimensional distance from the wall $y+<5$, (where $y+$ is the distance y to the wall, non dimentionalized with the friction velocity u_τ and kinematic viscosity v). This is needed in order to correctly resolve the viscous boundary layer in flows with high Re numbers. The models were contained in a near volume block of L x W x H = 2 x 2 x 1.5m meshed with polyhedral meshing. A structured grid with a greed refinement in the wake area was used to model the rest of the domain. The near-model volume was patched with the rest of the domain using the overset mesh technique implemented in STARCCM+. The overlap region between the near model mesh and the domain mesh was chosen to me 10cm. Three different surface meshes were used in a preliminary test in order to ensure a grid independent solution: a reference mesh consisting of 6.1million cells approximately, a coarse grid consisting of 3.1million approximately and a fine grid consisting of 12million cells approximately.

3.3 Boundary Conditions

Standard boundary conditions suggested in the STARCCM+ guide were used for the current simulation (Cd-ADAPCO, 2015). A uniform flow inlet was used at the inlet. For the oulet, assuming the outlet pressure known and equal to the atmospheric pressure, and being the exact details of the flow distribution unknown a pressure oulet boundary condition was used. Symmetrical boundary conditions were used in sides, top and bottom of the domain assuming that on the two sides of the boundary, same physical processes exist. With symmetrical boundary condition, all the variables have same value and gradients at the same distance from the boundary and no flow across boundary and no scalar flux across boundary. Even if this simplification could be considered acceptable, one has to be aware that the numerical domain is simplified with the real wind tunnel. In particular, this assumption leads to the fact that friction at the walls, with the direct consequence of boundary layer growth, is neglected and blockage effects are not considered (Chung, 2002). The model surface was modelled as a smooth wall surface with no slip conditions.

3.4 Solver Settings and Turbulence Modelling

The URANS turbulent flow solver implemented in STARCCM+ was used for the simulations and the k-ω Menter SST turbulence model was used for the simulations. A preliminary comparative study using the standard one equation Spalart Allmaras (SA) (Spalart, 2000) and the two equations k-ε model (Launder and Sharma, 1974) and the k-ω Menter SST (Menter, 1994) models was carried out and no noticeable differences between the use of the three models were found. Even if it is common knowledge that that no single turbulence model can be considered superior for all classes of problems and thus the choice of turbulence model often depends on considerations such as the physics embedded in the problem, the level of accuracy required and the available computational resources, the choice was made based on comparisons carried out by other authors. The SA does not accurately compute fields that exhibit shear flow, separated flow, or decaying turbulence. Its advantage is that it is quite stable and shows good convergence. K-ε does not accurately compute flow fields with adverse pressure gradients, strong curvature to the flow, or jet flow. The k- ω Menter SST model does not use wall functions and tends to be most accurate when solving the flow near the wall. Furthermore, SST model also enables to capture the vortex structures developing in the wake region. For this reason, since large separation and

vorticity is expected in the present test, the k-ω SST model was chosen (Zaïdi et al., 2010; Wilcox, 2006).

4 RESULTS AND DISCUSSION

4.1 Mannequin Models

The digital scanned model was positioned in the numerical wind tunnel in order to correctly reproduce the experiments position. The same simulation was carried out at six different wind speeds in order correctly replicate the wind tunnel experiments and verify if the velocity could influence the drag area.

4.1.1 Validation Against Experiments (Jersey on)

Figure 3: Mannequin model in the wind tunnel (left) and 3D laser scanned model (right).

Table 1: Comparison between experiments and simulations for the mannequin with jersey on.

Speed	[m/s]		9.53	11.2	13.09	14.93	16.97	18.72
$C_D A$		CFD	0.109	0.107	0.105	0.108	0.106	0.106
	[m^2]	EXP	0.098	0.098	0.097	0.096	0.096	0.095
Error	[%]		10.9	8.8	8.4	11.9	10.4	11.3
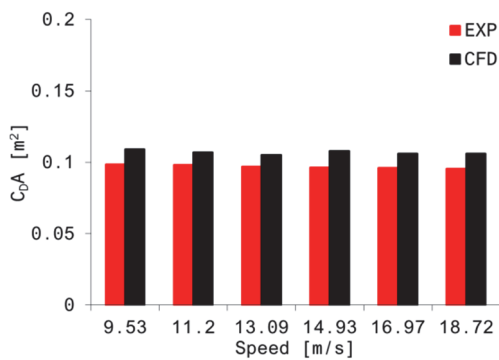
Figure 4: $C_D A$ values at different speeds for the mannequin with the jersey on for experiments (red) and simulations (black).

The results show that CFD simulations consistently match experiments at different wind speeds with an error between simulations and experiments in the order of 10% which can considered to be a good agreement (Blocken et al., 2013). The results clearly show that the $C_D A$ parameter is constant at different wind speeds allowing further simulations to limited to a single speed.

4.1.2 Effect of Jersey on the Surface

Two different configurations of the model were simulated (with and without jersey) in order to evaluate how the jersey could influence the overall drag. The test was carried out at 14.93m/s with the assumption that the drag coefficient would be constant at different wind speeds. Grooves and irregularities due to joints and mannequin construction were present on the model without jersey while these surface irregularities were either covered or smoothed in the scanned model with the jersey on (see Figure 5). In particular bumps and imperfections on the back and shoulder area can be seen in the Figure 5b while these imperfections are smoothed out in the model shown in Figure 5a
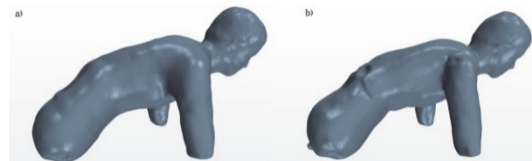
Figure 5: 3D scanned model a) model with jersey on. b) model without jersey.

The measured drag from the mannequin without jersey resulted to be higher than the measured drag from the mannequin with jersey on Figure 6.

Figure 6: Experimental results from the mannequin test with and without jersey.

The comparison between CFD and experiments presented in Figure 7 shows the same trend seen in Figure 6 and the main conclusion is that placing a jersey on the model surface affects the flow around reduces drag.
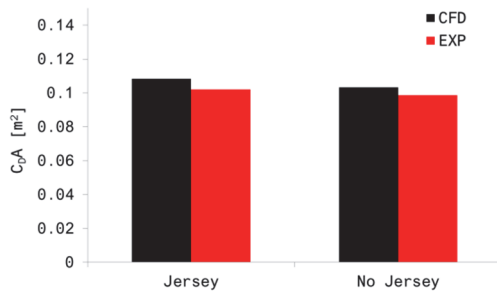
Figure 7: C_DA values from experiments (red) and simulations (black) for the mannequin model with and without jersey at 14.93m/s.

The irregular surface on the plain model creates low pressure zones that induce separation and recirculation of the flow with a consequent increase of pressure drag (Figure 8). In particular, it can be seen in in Figure 8b the wake area is larger than in Figure 8a. A high pressure area on the side of the model without jersey is also present while the same effect is not visible on the model with the jersey on.
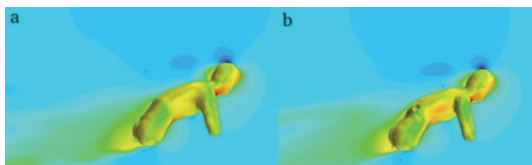
Figure 8: Pressure contour plots on a) the mannequin with jersey on and b) mannequin without jersey.

The same findings can be seen when plotting the friction lines on the model. A recirculation area on the side of the model can be seen. This recirculation area is generated by the groove in the shoulder region where the arm is attached to the torso. From Figure 9 it can also be seen that the flow on the arm separates differently on the model with jersey and on the model without jersey.
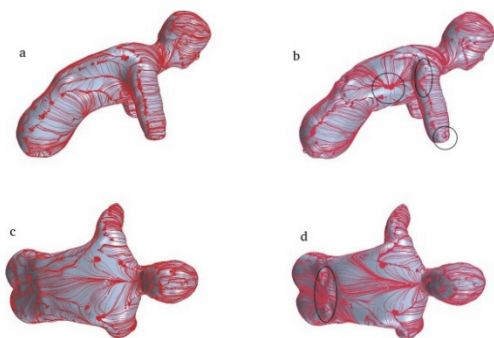
Figure 9: Friciton lines on the model with jersey (a,c) and without jersey (b,d).

Similar conclusions come also from figure 10

where the vorticity field around the model is represented for visualization purposes. In the model with no jersey Figure 10b, the groove in the shoulder joint creates a vortex that develops and reattaches on the side of the model while the irregularities in the back induce separation.
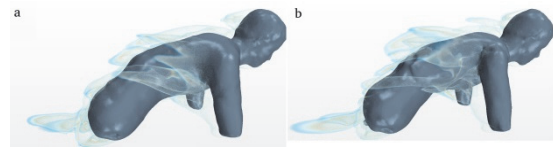
Figure 10: Vorticity field around the mannequin model. a) with jersey b) without jersey.

4.2 Cyclist

4.2.1 Validation Against Experiments (Dropped Position)

Experiments were available only for the cyclist in dropped position. The drag of the bare athlete with no bike was obtained subtracting the drag measured for the bare bike from the drag measurements from the bike+cyclist test. While the experiments were carried out at three different wind speeds, a single CFD simulation at 13.09 m/s was carried out assuming the C_DA from CFD to be independent from the wind speed.

The results from the CFD simulation match the experiments with an error of 10% and the simulated drag area C_DA is consistently higher than the measured one. The over prediction of the aerodynamic drag is a known problem in CFD simulations and it is directly linked to the turbulence modelling (Blocken et al., 2013). The standard turbulence models are in fact not able to correctly simulate the vortices in the recirculation regions and they often tend to keep the large structures without correctly resolving the smaller structures that are responsible of the vortex breaking mechanism, leading to an over prediction of the total drag.
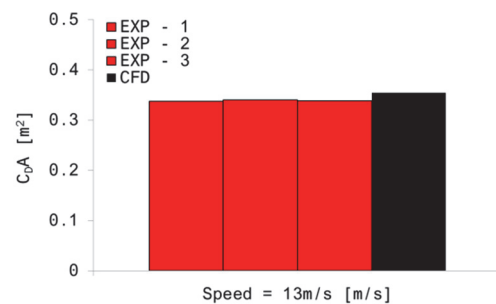
Figure 11: C_DA values for the cyclist model from simulations (black) and experiments (red).

Figure 12 illustrates the vorticity field around the cyclist and the pressure field on the cyclist. The interaction between the different body parts can be seen in Figure 12a where the vortices generated by the arms directly interact with the athlete trunk. Figure 12b gives an overview of the area where separation might occur. The low pressure areas (blue color) are areas where the flow is detached. Large vortices are usually generated from these areas leading to an increase in total drag. Major attention to these areas is then important when designing a low drag suit.

Figure 12: Vorticity field around the full model. And pressure contour plots on the model.

5 CONCLUSIONS

CFD simulations proved to be a useful tool and the results consistently matched the experimental results with an over prediction estimated to be around 10%. If on one side experiments are still needed, especially for surface modifications and dynamic testing, CFD could give a much better insight of the pressure and force distribution on the body. CFD could then be a good complementary tool to use in parallel with wind tunnel testing

REFERENCES

Blocken, B., Defraeye, T., Koninckx, E., Carmeliet, J. & Hespel, P. 2013. Cfd simulations of the aerodynamic drag of two drafting cyclists. *Computers & Fluids,* 71, 435–445.

Brownlie, L. 1992. *Aerodynamic characteristics of sports apparel.* Simon fraser university.

Brownlie, L., Gartshore, M., Mutch, B. & Banister, B. 1987. Influence of apparel on aerodynamic drag in running. *The Annals of Physiological Anthropology,* 6, 133-143.

Brownlie, L., Kyle, C. R., Carbo, J., Demarest, N., Haber, E., Macdonald, R. & Nordstrom, M. 2009. Streamlining the time trial apparel of cyclists: the nike swift spin project. *Sports technology,* 1-2, 53-60.

Cd-adapco 2015. Starccm+ user guide.

Chung, T. J. 2002. *Computational fluid dynamics,* Cambridge University Press.

De Groot, G., Sargeant, A. & Geysel, J. 1995. Air friction and rolling resistance during cycling. *Medicine and science in sports and exercise,* 27, 1090–1095.

Debraux, P., Grappe, F., Manolova, A. V. & Bertucci, W. 2012. Aerodynamic drag in cycling: methods of assessment. *Sports biomechanics,* 10, 197–218.

Defraeye, T., Blocken, B., Koninckx, E., Hespel, P. & Carmeliet, J. 2010a. Aerodynamic study of different cyclist positions: CFD analysis and full-scale wind-tunnel tests. . *Journal of biomechanics,* 43, 1262-1268.

Defraeye, T., Blocken, B., Koninckx, E., Hespel, P. & carmeliet, j. 2010b. Computational fluid dynamics analysis of cyclist aerodynamics: performance of different turbulence-modelling and boundary-layer modelling approaches. *Journal of Biomechanics,* 43, 2281-2287.

Defraeye, T., Blocken, B., Koninckx, E., Hespel, P. & Carmeliet, J. 2011. Computational fluid dynamics analysis of drag and convective heat transfer of individual body segments for different cyclist positions. *Journal of Biomechanics,* 44, 1695–701.

Di Prampero, P. E. 2000. Cycling on earth, in space and on the moon. *European Journal Applied of Physiology,* 82, 345–360.

Hanna, R. K. 2002. Can CFD make a performance difference in sport? *In:* Haake SJ, E. (ed.) *The Engineering of Sport 4.* Oxford: blackwell science.

Launder, B. E. & sharma, B. I. 1974. Application of the energy dissipation model of turbulence to the calculation of flow near a spinning disc. *Letters in Heat and Mass Transfer,* 1, 131-138.

Lecrivain, G., Slaouti, A., Payton, C. & Kennedy, I. 2008. Using reverse engineering and computational fluid dynamics to investigate a lower arm amputee swimmer's performance. *Journal of Biomechanics,* 13, 2855–2859.

Lukes, R. A., S.B., C. & S.J, H. 2002. The understanding and development of cycling aerodynamics. *Sports engineering,* 8, 59–74.

Menter, F. R. 1994. Two-equation eddy-viscosity turbulence models for engineering applications. *Aiaa journa,* 32, 1598–1605.

Minetti, A. E., Machtsiras, G. & C., M. J. 2009. The optimum finger spacing in human swimming. *Journal of biomechanics,* 42, 2188–90.

Oggiano, L. & Sætran, L. 2012. Experimental analysis on parameters affecting drag force on speed skaters. *Sports technology,* 3, 223-234.

Oggiano, L., Sætran, L., Leirdal, S. & Ettema, G. 2008. Aerodynamic optimization and energy saving of cycling postures for international elite level cyclists. *The Engineeeing of Sport 7,* 597-604.

Oggiano, L., Troynikov, O., Konopov, I., Subic, A. & F., a. 2009. Aerodynamic behaviour of single sport jersey fabrics with different roughness and cover factors. *Sports Engineering,* 12, 1-12.

Spalart, P. R. 2000. Strategies for turbulence modelling and simulations. *Int. J. Heat Fluid Flow* 21 (3), 252–

263.

Underwood, L. 2012. *Aerodynamics of track cycling.* Doctor of philosophy, the University of Canterbury.

Underwood, L. & Jermy, M. C. Fabric testing for cycling skinsuits. 5th Asia-pacific congress on sports technology (APCST), 2011 Melbourne. 350–356.

Wilcox, D. C. 2006. *Turbulence modelling for CFD,* la Canada, California, USA.

Zaïdi, H., Fohanno, S., Taïar, R. & Polidori, g. 2010. Turbulence model choice for the calculation of drag forces when using the CFD method. *Journal of Biomechanics,* 10, 405-11.